Geomorphology 413 (2022) 108362

Contents lists available at ScienceDirect

Geomorphology

journal homepage: www.journals.elsevier.com/geomorphology

Effects of grain composition on the stability, breach process, and breach parameters of landslide dams

Danyi Shen [a], Zhenming Shi [a], Hongchao Zheng [a,*], Jiangtao Yang [a], Kevin J. Hanley [b]

[a] Key Laboratory of Geotechnical and Underground Engineering of the Ministry of Education, Department of Geotechnical Engineering, College of Civil Engineering, Tongji University, China

[b] School of Engineering, Institute for Infrastructure and Environment, The University of Edinburgh, United Kingdom

ARTICLE INFO

Keywords:
Landslide dams
Grain composition
Failure mode
Breach process
Breach parameters

ABSTRACT

The sudden breach of a landslide dam seriously threatens the safety of people and property downstream. The failure mechanism of landslide dams is significantly affected by the grain size distribution of the dam material. In this study, a series of experiments are conducted to investigate the effects of grain composition on the stability, breach process, and breach parameters of landslide dams. The results show that dams remain stable with seepage for a coarse-dominated dam, fail by overtopping along with piping for a fines-dominated dam, and fail by overtopping alone for a balanced-composition dam. The failure mode is regulated by the composition of dam material, stress condition and hydraulic gradient. Backward erosion occurs for dams with fines contents <5 % due to the movement of debris, during which the width:depth ratio of the cross section first decreases and then increases. By contrast, for dams with fines contents higher than 15 %, headcutting occurs and a step-pool structure develops because the small grains are more easily washed away than the coarse grains. In this scenario, the width:depth ratio first increases and then decreases. Dam longevity nonlinearly increases with increasing fines content. The breach hydrography changes from a single peak to multiple peaks with increasing fines content, and the peak discharge is sensitive to the median diameter of dam material. In addition, the breach degree, defined as the ratio of the releasing potential energy (total potential energy minus the residual potential energy) to the total potential energy of the lake upstream of the landslide dam, is controlled by this median diameter. This study improves our understanding of failure mechanisms and aids the hazard assessment of landslide dams.

1. Introduction

Landslide dams are usually formed by river blockages with massive amounts of material from avalanches, landslides, or debris flows triggered by rainstorms, rapid snowmelt, or earthquakes (Dong et al., 2009; Zheng et al., 2021a). Throughout history, breaches of landslide dams have caused catastrophic floods, posing great threats to lives and infrastructure downstream (Shen et al., 2020). For instance, the 2008 Tangjiashan landslide dam breached with a peak outflow rate of 6500 m^3/s, threatening Mianyang city (85 km downstream) and >2.5 million people (Fan et al., 2012). Another example is the breach of the 2018 Baige landslide dam, causing a flash flood with a peak discharge of 33,900 m^3/s, resulting in the homelessness of >25 thousand people (Zhang et al., 2019).

Compared with man-made dams, landslide dams are composed of mixtures of clay, sand and rock with grain sizes ranging from microns to meters (Chang and Zhang, 2010; Ruan et al., 2021). Depending on the formation process, the grain compositions of landslide dams can differ significantly, which determines breach characteristics like peak discharge and breach time. For example, >70 % of the debris comprising the Hsiaolin landslide dam was silt or sand with grain diameters <2 mm; this dam breached within 1 h and had a peak discharge of 70,649 m^3/s (Li et al., 2011). By contrast, only about 15 % of the grains comprising Xiaogangjian landslide dam had grain diameters <2 mm; this dam failed one month after formation with a peak discharge of 3000 m^3/s (Chen et al., 2018). This comparison shows the importance of studying the effect of grain composition on the breach mechanism.

Many research studies have been conducted to investigate the influence of the grain composition on the stability of landslide dams (Coleman et al., 2002; Morris et al., 2008; Zhu et al., 2020). According to

* Corresponding author.
E-mail address: 1410274@tongji.edu.cn (H. Zheng).

https://doi.org/10.1016/j.geomorph.2022.108362
Received 15 February 2022; Received in revised form 24 May 2022; Accepted 27 June 2022
Available online 30 June 2022
0169-555X/

statistical analysis, rock-type landslide dams usually maintain stability better than soil-type and debris-type dams (Zheng et al., 2021b). Both field surveys and laboratory experiments show that landslide dams with different grain compositions can fail by piping, overtopping, or slope slide. According to Okeke and Wang (2016), and Wang et al. (2018), if the dam material has $D_{15}/D_{85} > 5$ and a high content of fines ($d < 0.063$ mm), it is usually easy to form a complete seepage path leading to piping failure. Chen et al. (2015) claims that the failure mode is controlled by the permeability and strength of the dam material. Overtopping failure is more likely to occur for dams with small permeability coefficients and high soil strength, while slope failure caused by internal instability is possible with large permeability coefficients and weak soil strength. The effects of grain composition on the failure mode have been analyzed only for a specified grain diameter; the effects of varying the proportions of silt, sand, and gravel, for example, still have not been explored.

Analyses of the breach processes of landslide dams demonstrate that overtopping processes can be divided into surface erosion, backward erosion, and water-material rebalance based on longitudinal section evolution (Zhou et al., 2019; Zhong et al., 2021). The downstream dam slope is gentle when the dam material contains few fines, while the downstream dam slope is steep and "V"-shaped when the dam material contains a large proportion of fines (Yang et al., 2015). A breach develops faster with increasing median diameter, although the presence of large grains in the dam material slows down breach development (Ermini and Casagli, 2003; Schmocker et al., 2014). The breach width enlarges as debris from the sides of the breach drops into the breach channel and is carried away (Rozov, 2003). The shape of the breach channel changes from trumpet-shaped to dumbbell-shaped during dam breaching, and the enlargement rate of breach width depends on the erosion rate of dam material at the breach sides (Zhang et al., 2021). The erosion rate increases faster in the vertical direction than in the lateral direction as fines are added (Jiang et al., 2018). Although the effects of dam material on the breach process have been explored from a qualitative perspective, the correlation between breach development and grain composition has not been studied in detail.

The commonly studied breach parameters of landslide dams are the breach discharge, breach duration, and residual dam height. Yang et al. (2015) proposes that the peak discharge increases with decreasing median diameter but increasing fines content, while the breach duration increases with increasing median diameter but decreasing fines content. Mei et al. (2021) reveals that the grain size distribution controls the residual dam height after a dam breaches. Jiang et al. (2018) and Zhao et al. (2019) claim that a residual dam height exists for most landslide dams with large boulders or unjointed rock masses towards its base. Jiang and Wei (2019) observes that the residual dam height decreases with the increase of initial soil moisture. Zhong et al. (2020) analyzes the grain composition and residual dam height after the breach of a specific landslide dam. Despite these prior studies, the effects of grain composition on the breach parameters, especially a reasonable parameter to represent the residual dam, need to be further studied.

A series of experiments under controlled conditions are conducted to analyze the effects of grain composition on the stability, breach process, and breach parameters of landslide dams. The structure of this study is as follows. First, experimental flume setup, grain composition, and experimental design are described. Then, the observations of stability and breach processes of dams are presented. Based on these observations, the effects of grain composition on breach parameters, including peak discharge, breach duration, and breach degree are investigated. Finally, the stability evaluation of dams, the erodibility of dam materials with different grain compositions, and the comparison of tested dams and landslide dams in the field are discussed.

2. Materials and methods

2.1. Experimental setup

The experiments were conducted in a rectangular flume system located at Tongji University. The flume system consisted of a water injection pump, water tank, flume, and collection pool (Fig. 1). The water injection pump combined with an electromagnetic flowmeter was installed upstream of the water tank to provide the required inflow rate. The water tank, with a length of 0.42 m, a width of 0.68 m, and a height of 0.48 m, was used to provide a smooth entrance flow into the flume. The flume had a length of 5.0 m, a width of 0.4 m, and a height of 0.4 m. The sidewalls of the flume were made of organic tempered glass so that the breach processes of model dams could be observed. The flume bottom was horizontal because the longitudinal gradients of dams in the field are generally small, e.g., 0.006 for Tangjiashan landslide dam (Peng et al., 2014). The water at the downstream end of the flume flowed freely into the collection pool and thus the water level downstream of the dam was kept at nearly zero.

Four video cameras (GZ-R10BAC, JVC, 1920 × 1080 pixel) with a sampling frequency of 25 Hz were used to record the breach processes of dams from four directions (Fig. 1(a)). Camera 1 combined with a 40 cm steel tape was placed upstream of a dam to record the change of water level, allowing the breach discharge to be calculated using the continuity equation. Camera 2 was located at the side of the flume to collect the breach depths during the failures of dams. Camera 3 and a steel tape were suspended above a dam to record and measure the breach width, and camera 4 was placed downstream of a dam to record the development of the breach channel.

2.2. Experimental materials

Eleven grading curves were chosen for the dam materials based on 42 landslide dams in the Northern Apennines (Casagli et al., 2003). As shown in Fig. 2, each grading curve had different contents of silt, sand, and gravel. The grain sizes of the silt, sand and gravel particles were classified same as Zhou et al. (2019). The grain composition was divided into three typical types denoted as coarse-dominated, fines-dominated, and balanced-composition according to the silt and gravel content. The coarse-dominated debris contained >80 % gravel, while the fines-dominated debris was defined as having >45 % silt. The balanced-composition debris had silt and gravel contents that vary between the coarse-dominated and fines-dominated debris. The classification was different from the standard engineering classification of soils. The median grain sizes d_{50} of fines-dominated debris were 0.05–0.07 mm, which were smaller than the values for the balanced-composition debris (0.87–8.82 mm) and coarse-dominated debris (8.77–13.26 mm) (Table 1). The particles with sizes below 0.075 mm were deemed to be fine particles, and the particles larger than 0.25 mm were deemed to be coarse particles (Tian et al., 2020). The fines content p ($d < 0.075$ mm) for the eleven grain compositions ranged from 1.02 % to 55.86 %.

Each dam material was prepared by mixing silt, silica sand, and gravel according to the required grain composition (Fig. S1). The geotechnical properties of each dam material were measured (Table 1). The maximum dry density ρ_{dmax} of a dam material, used to calculate the weight of dam debris under a controlled degree of compaction, was obtained from the proctor compaction test (Ministry of Construction of the People's Republic of China, 2001). The values of ρ_{dmax} of the dam materials ranged from 1980 kg/m^3 to 2410 kg/m^3. The angle of repose φ, which reflected the rolling and sliding friction of a dam material, was measured using rectangular container tests (Zhou et al., 2002). Each dam material was tested five times to obtain an average φ value. The values of φ of the fines-dominated debris were smaller than those of the balanced-composition debris and coarse-dominated debris. The saturated permeability coefficients k of the dam materials were obtained according to Darcy's law.

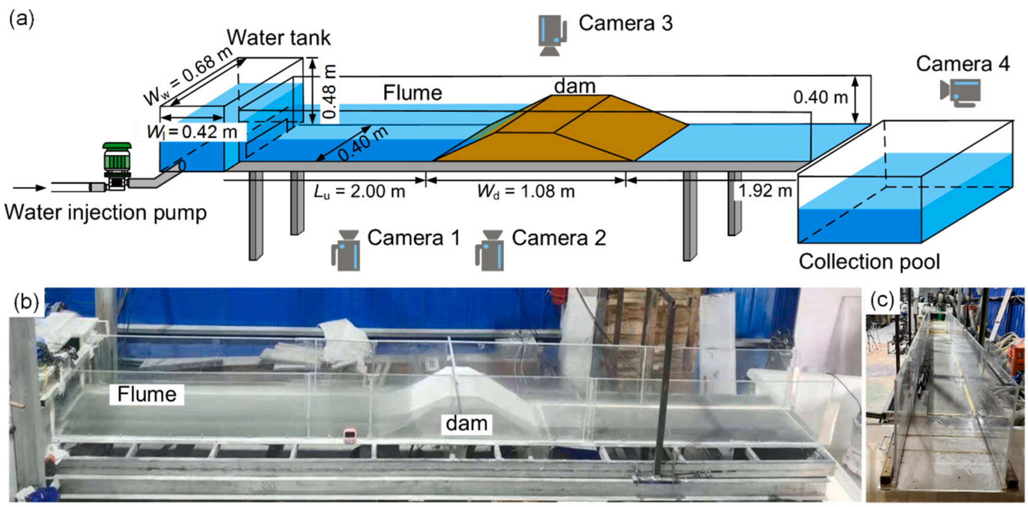

Fig. 1. Schematic diagram of experimental apparatus: (a) A sketch of the experiment setup; (b), (c) Photographs of the experimental flume.

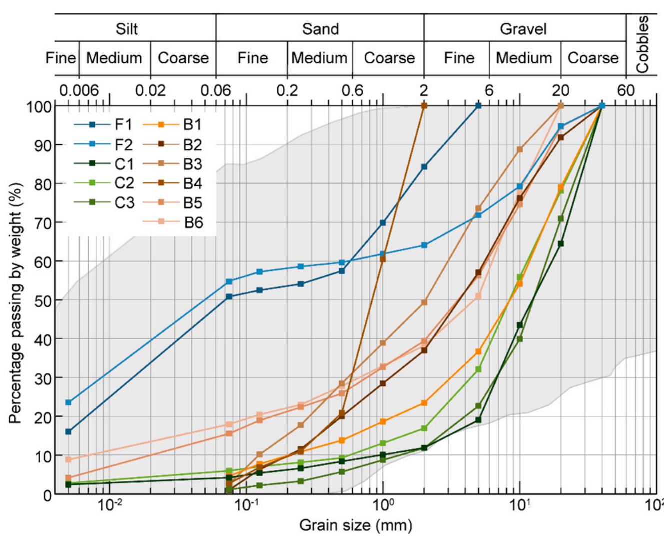

Fig. 2. Grading curves of the debris materials used in the model dams. Note: the gray area is the grain composition of 42 landslide dams in the Northern Apennines reported by Casagli et al. (2003).

2.3. Experimental design

The experiments were designed to explore the effects of grain composition on the stability, breach process, and breach parameters of dams. The dam geometry, e.g., dam height, crest width, and breach channel size, and the inflow rate were kept constant in the experiments. In total, eleven experiments with different dam materials were conducted.

The geometrical parameters of landslide dams vary significantly. Thus, this study did not select a specific dam as a prototype. As shown in Fig. 3, each dam was modeled as a trapezoidal prism with a crest width W_t of 12 cm, a bottom width W_d of 108 cm, a height H_d of 24 cm, and a transverse length of 40 cm. The upstream and downstream slopes of the dams were fixed at 26.6° because the slopes of natural landslide dams are in the range 11–45° (Zheng et al., 2021b). The dam shape coefficient ($V_d^{1/3}/H_d$), the ratio of dam height to dam bottom width (H_d/W_d), and the lake shape coefficient ($V_l^{1/3}/H_d$) were 1.61, 0.22, 2.56, respectively, where V_d and V_l are dam volume and lake volume. These dimensionless numbers were within the ranges for natural landslide dams reported by Zhou et al. (2019), indicating the model satisfies scaling laws. A triangular initial breach was excavated at the side of each dam to ensure that the overflow started at the same position for each experiment. The initial breach was 4 cm in depth and 5 cm in top width. Throughout each experiment, the inflow rate remained constant at 1 L/s. The hydrodynamic coefficient ($(Q_{in}T_r)^{1/3}/H_d$) was 0.42, where Q_{in} is the inflow rate

Table 1
Summary of geotechnical properties of dams.

Dam material	Test	ρ_{dmax} (kg/m^3)	d_{50} (mm)	Silt (%)	Sand (%)	Gravel (%)	p (%)	C_u	C_c	φ (°)	e	k (10^{-4} m/s)
Coarse-dominated	C1	2400	13.11	3.79	8.06	88.15	4.17	18.40	3.03	44.3	0.57	188
	C2	2370	8.77	5.26	11.60	83.14	5.95	19.87	2.98	39.8	0.59	124
	C3	2250	13.26	0	11.78	88.22	1.13	11.63	2.18	39.0	0.67	248
Fines-dominated	F1	2120	0.07	47.36	36.90	15.74	50.82	120.73	0.36	19.0	0.82	0.81*
	F2	2200	0.05	53.45	10.59	35.96	55.86	116.78	0.12	19.8	0.71	0.28*
Balanced-composition	B1	2410	8.82	0	23.45	76.55	4.56	57.11	4.53	38.3	0.56	135
	B2	2360	3.95	0	36.95	63.05	1.02	26.95	1.13	35.0	0.59	7.22
	B3	2200	2.08	0	49.32	50.68	2.59	26.78	0.80	36.8	0.71	6.61
	B4	1980	0.87	0	100	0	2.68	4.50	1.72	31.3	0.90	1.77
	B5	2350	4.77	15.96	22.21	61.83	17.90	474.49	5.43	25.0	0.60	1.02
	B6	2270	3.89	13.09	26.30	60.61	15.53	146.96	2.64	21.8	0.66	1.25

Note: ρ_{dmax} is the maximum dry density of the dam material. d_{50} is the median diameter. p is the fines content ($d < 0.075$ mm). C_u and C_c are the uniformity coefficient and curvature coefficient of the grading curve, respectively. φ is the angle of repose. e is the void ratio. k is the saturated permeability coefficient of dam material. * The value was calculated by $k = K\frac{\rho_w g}{\mu}$, where $K = d_{50}^2\left(\frac{e}{1+e}\right)^3/180\left(1-\frac{e}{1+e}\right)^2$ (Goren et al., 2010), ρ_w is the density of water (1000 kg/m^3), g is the gravitational acceleration (9.8 m/s^2), μ is the dynamic viscosity of water (1×10^{-3} Pa·s).

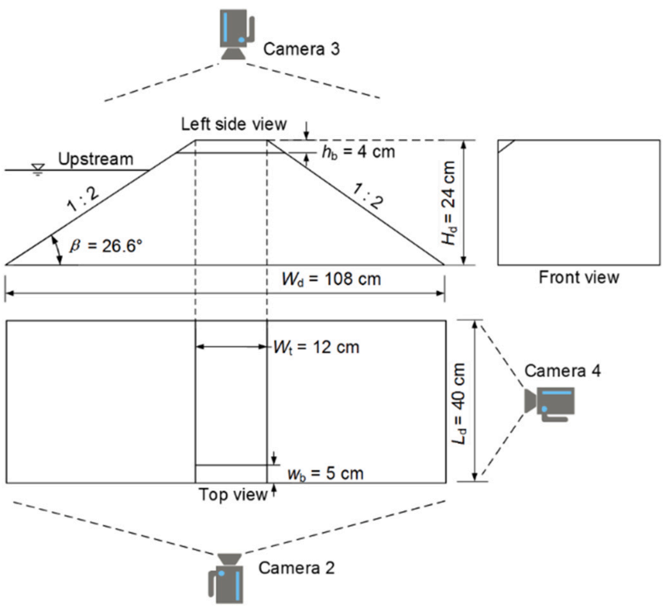

Fig. 3. Layout of dam model.

and $T_r = 1$ s. The value was in the range for natural landslide dams determined by Li et al. (2021), indicating the inflow rate of the model dam satisfies scaling laws (Fig. S2).

2.4. Experimental procedure

The detailed experimental procedure is listed as follows:

(1) Flume preparation. Transparent grid paper (1 cm × 1 cm) was pasted on the sidewalls, and the contours of the dam were drawn in the preset shape with an oil pencil.
(2) Dam material preparation. After obtaining the maximum dry density by compaction test, the total mass of the dam was calculated based on the controlled degree of compaction of 70 %. Weights of each fraction were then determined. Different components of the dam material were adequately mixed through repeated stirring.
(3) Dam construction. To provide enough backwater area, the model dam was built 2 m away from the water tank (Fig. 1). The dam was constructed in 4 layers, each layer with a thickness of 6 cm. Each layer was uniformly compacted by a wooden board. After the dam was constructed, a triangular notch (w_b x h_b = 5 cm × 4 cm) was excavated on the dam crest, adjacent to a side wall.
(4) Experimental process. Four cameras were installed as aforementioned to record the whole experiment. The inflow rate was controlled at 1 L/s by an electromagnetic flowmeter. The experiment stopped after the dam breached or remained stable for 3 h.
(5) Data processing. The stability of each dam was obtained from the recorded snapshots. The outflow discharge Q_{out} was calculated from the water level upstream of the dam:

$$Q_{out} = Q_{in} - \frac{V(t+\Delta t) - V(t)}{\Delta t} \tag{1}$$

where Q_{in} is the inflow rate, $V(t + \Delta t)$, $V(t)$ are the volumes of the reservoir after the dam overtopped at time $t + \Delta t$, and at time t.

At time t, the volume of the reservoir is calculated according to the geometric relationship

$$V(t) = W_l \times W_w \times H_w(t) + \frac{1}{2}H_w(t) \times [2L_u + H_w(t)cot(\beta)] \times W_f \tag{2}$$

where W_l and W_w are the length and width of the water tank, $H_w(t)$ is the water level upstream of the dam at time t, L_u is the distance from the upstream dam site to the water tank, β is the upstream slope angle of the dam, W_f is the width of the flume.

3. Experimental results

In this section, the stability of coarse-dominated (C1–C3), fines-dominated (F1 and F2), and balanced-composition (B1–B6) dams are analyzed. Then overtopping processes of dams with different grain compositions are studied (B1–B6). Finally, the effects of grain composition on breach parameters of the dams (F1, F2, B1–B6) are investigated.

3.1. Effects of grain composition on dam stability

3.1.1. Stable dams

The dams with coarse-dominated debris (C1–C3) remained stable throughout the experiments. Taking test C1 as an example, the water level upstream rose slowly and a seepage path was formed due to the high permeability of the dam material (Table 1). The water began to seep near the toe of the downstream face of the dam when the upstream water level H_w reached 5.8 cm. Some small grains with diameters <0.5 mm migrated from the seepage path as individual grains (Figs. 4(a), (b)). At this time, the seepage rate was smaller than the rate of inflow, resulting in the continuous rise of the water level upstream and the increase of seepage line gradient (Figs. 4(c), (d)). After water entered the breach channel and formed an overflow, small grains on the downstream slope face were taken away but the dam remained stable (Fig. 4(e)). The upstream water level remained at 22.1 cm when the inflow and outflow reached an equilibrium. The outflow water gradually became transparent (Fig. 4(f)).

For coarse-dominated debris, the gravel content was more than four times that of silt and sand, indicating that the dam material was mainly composed of gravel grains in contact with each other. The sand and silt partially filled the pores between gravel grains (Fig. S3). According to Shire et al. (2014), the fines sat loose and understressed within the voids when $p < 24$ %, and they were unconnected to the stress transfer matrix. Therefore, the fines migrated through the seepage path easily, and their loss did not reduce the stability of the dam.

Considering grains on the downstream slope were subjected to both seepage and overtopping flows, this may cause their incipient motion. Assuming the dam body had a uniform void ratio and grains were spheres, five forces act on a grain: the drag force F_d, the uplift force F_l, submerged weight force F_w, the seepage force F_p, and resistance force due to friction F_r (Fig. 5) (Lu et al., 2012).

$$F_d = \frac{\pi}{8}C_D\rho_w u_b^2 d^2 \tag{3}$$

where C_D is the drag coefficient, ρ_w is the density of water, u_b is the flow velocity acting on the grain, d is the equivalent diameter of the grain.

$$F_l = \frac{\pi}{8}C_L\rho_w u_b^2 d^2 \tag{4}$$

where C_L is the lift coefficient.

$$F_w = \frac{\pi}{6}(\rho_s - \rho_w)gd^3 \tag{5}$$

where ρ_s is the density of the grain (2650 kg/m^3), g is the gravitational acceleration.

$$F_p = \frac{\pi}{6}\rho_w gid^3(1+e) \tag{6}$$

where i is the hydraulic gradient for seepage. The resistance force F_r opposing motion, arising from friction, depends on F_w, F_l, and F_p:

$$F_r = \zeta\left[F_w cos\beta - F_l - F_p sin(\beta - \alpha)\right] \tag{7}$$

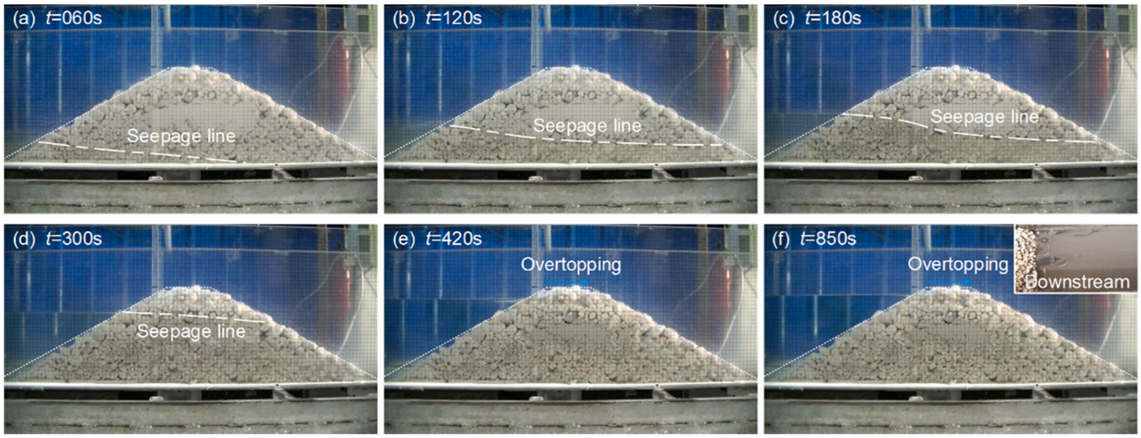

Fig. 4. Stability of the coarse-dominated dam in test C1.

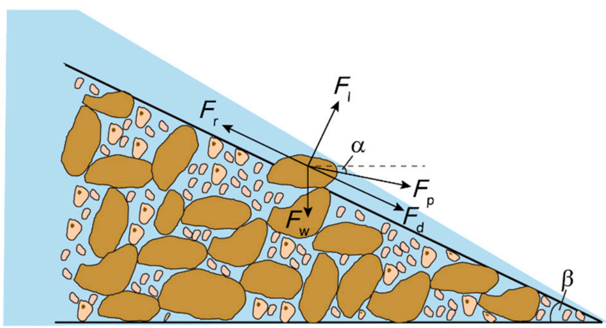

Fig. 5. Forces acting on grains lying on the downstream slope.

where $\zeta = \tan\varphi$ is the static friction coefficient. In the grain threshold condition, the force components of F_d, F_w, and F_p should be equal to F_r. Therefore,

$$F_d + F_P cos(\beta - \alpha) + F_w sin\beta = F_r \tag{8}$$

Based on Eqs. (3)–(8), the maximum diameter d_m of a grain that is moved by the seepage flow and overtopping flow is expressed as

$$d_m = 0.75\frac{u_b^2}{g}\frac{(C_D + C_L tan\varphi)}{\left(\frac{\rho_s}{\rho_w} - 1\right)(cos\beta tan\varphi - sin\beta) - i(1+e)[sin(\beta - \alpha)tan\varphi + cos(\beta - \alpha)]} \tag{9}$$

where α is the angle between the seepage force and the horizontal, and β is the angle of the downstream slope of the dam.

For the dam in test C1, with $u_b = 0.13$ m/s, $\rho_s = 2650$ kg/m^3, $\beta = 26.6^\circ$, $C_D = 0.4$, $C_L = 0.04$, and maximum $\alpha = 6.65^\circ$, $d_m = 1.22$ mm based on Eq. 9. This value is smaller than the grain diameter of fine gravel and close to the observed particle size. The grains with diameters <1.22 mm account for only 10.1 % of the dam material. This further indicates that the loss of grains does not lead to the instability of the dam due to the weak transport induced by seepage and overtopping.

3.1.2. Dams failed due to overtopping along with piping

Fines-dominated debris dams in tests F1 and F2 failed due to overtopping along with piping. Taking test F1 as an example, the seepage line developed slowly due to the low permeability caused by the large amount of silt (Fig. 6(a)). After water propagated through the dam's breach channel, a scour pit, which was determined by the outflow condition and dam material, occurred near the toe of the dam downstream (Zhong et al., 2021) (Fig. 6(b)). The Reynolds number of outflow water changed from 990 to 28277 after overtopping, indicating that the outflow in test F1 changed from laminar flow to turbulent flow. An irregular seepage path of length 4 cm formed at a height of 10 cm on the upstream slope when $H_w = 23.5$ cm. Headcutting occurred and the downstream slope angle increased continuously due to the strong erosion caused by the vortexes in the scour pit, while the dam height was almost unchanged (Fig. S4). This feedback mechanism reduced the seepage length and effective stress of the soil while maintaining a high seepage force, thus promoting the formation of piping (Fig. 6(c)). A complete pipe channel then formed (Fig. 6(d)). Some small grains, including silt, sand, and fine gravel, were detached and transported through the pipe channel which, in turn, broadened the diameter of the channel (Figs. 6(d) and (e)). The upstream water level dropped rapidly through the large pipe channel and then the overtopping stopped. The dam material above the pipe roof collapsed as the weight of overlying debris could not be supported. The blockage was washed away by overtopping water, resulting in the further reduction of dam height (Fig. 6(f)). The upstream water level of the dam eventually remained stable at 2.5 cm due to the formation of an armoring layer.

The silt content of the fines-dominated debris was >45 %, and the fines content p was >50 %. This indicates that most contacts in the dam were between fines, and the coarse grains were enveloped by fines (Vallejo and Mawby, 2000) (Fig. S3). In addition, the grading curves of fines-dominated debris were deficient in a certain grain size (Table 1, Fig. 2). According to Kenney and Lau (1985), if the mass fraction between grain sizes d and $4d$ is small, the grains of size d can pass through the skeleton formed by grains of size $4d$ and larger, and thus piping can readily occur. With $d = 0.075$ mm, the percentages of grains between 0.075 mm and 0.3 mm in tests F1 and F2 were 3.92 % and 2.91 %, respectively: a small mass fraction which is conducive to the loss of fines. It also indicated that the voids in the dam material were not overfilled, many fines carried only weak contact forces, and thus could be removed by hydraulic gradients (Shire et al., 2014). These results indicated that >50 % of grains can pass through the dam skeletons, so it was easy to form piping channels in these two dams.

Internal instability only occurs when the hydraulic gradient exceeds a critical threshold. The critical hydraulic gradient i_c is expressed as (Terzaghi, 1929)

$$i_c = \frac{\rho_s g - \rho_w g}{\rho_w g}\left(\frac{1}{1+e}\right) \tag{10}$$

For the dam in test F1, with $\rho_s = 2650$ kg/m^3, $i_c = 0.91$. The maximum hydraulic gradient reached 0.98 at $H_w = 23.5$ cm: much larger than the critical hydraulic gradient, and thus internal instability occurred in the dam.

3.1.3. Dams failed due to overtopping alone

The dams with balanced-composition debris (B1–B6) breached by

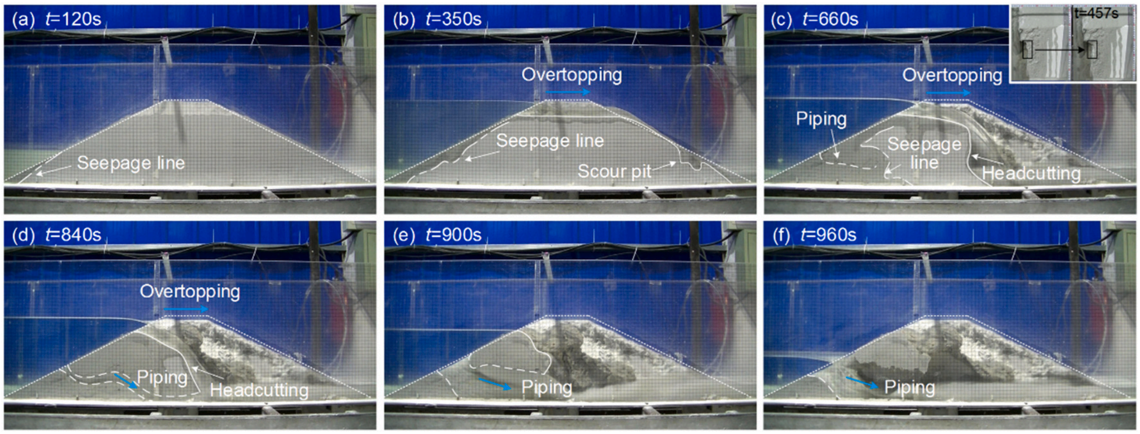

Fig. 6. Failure process of the fines-dominated dam in test F1.

overtopping. Taking test B1 as an example, water seeped through the toe of the downstream dam with $H_w = 9.1$ cm (Fig. 7(a)), which was larger than the corresponding value for the dam in test C1 (5.8 cm). Backward erosion occurred when $H_w = 23.4$ cm. Both slide and collapse intermittently occurred along the breach channel, but the volume was relatively limited (Figs. 7(b), (c)). Some coarse grains were rolled under the water flow and deposited near the toe of the downstream slope (Fig. 7(d)). The dam height decreased and lateral collapse occurred when the erosion reached the upstream face of the dam, which promoted the deepening and widening of the breach channel (Fig. 7(e)). During the breach, the Reynolds number of outflow water changed from 495 to 91320 in test B1. The breach channel in the cross section was nearly trapezoidal, and it was similar to an hourglass along the longitudinal section. An armoring layer was formed on the bottom of the breach to resist further erosion, before the inflow rate and outflow rate reached equilibrium (Fig. 7(f)).

For the balanced-composition debris, the contents of silt, sand, and gravel varied between the coarse-dominated and fines-dominated debris (Fig. S3). Except for the dam in test B4 composed of sand only, the contents of silt and sand in tests B1–B3, B5, and B6 accounted for 0–15.96 % and 22.21–49.32 %, respectively, and the gravel content accounted for 50.68–76.55 %. The seepage rate in test B1 (0.36 L/s) was smaller than the value in test C1 (0.75 L/s). Based on Eq. (9), the maximum diameter d_m of a grain that is taken away by the seepage flow and overtopping flow is 20.8 mm. This means >80 % of the dam material was washed away if the flow velocity remained at the maximum value. This was why overtopping failure occurred for the balanced-composition dams but not for the coarse-dominated dams. The critical hydraulic gradient i_c in test B1 was 1.06: much larger than the maximum hydraulic gradient (0.36) that was achieved during the test. Thus, piping did not occur for the balanced-composition dams but only for the fines-dominated dams.

3.2. *Overtopping process for balanced-composition dams*

3.2.1. *Longitudinal section evolution*

The breach processes of balanced-composition dams varied with fines content, even though all failed by overtopping. The dams in tests B1–B4 with fines contents <5 % breached through continuous backward erosion, layer by layer (Figs. 7, 8(a) and S5–S7). This backward erosion was due to exceeding the critical shear stress for incipient sediment movement on the downstream slope face after overtopping. Some coarse grains were deposited near the toe of each dam downstream. Subsequently, the dam height decreased as the backward erosion migrated to the upstream slope face. The downstream slope angle continuously reduced from 26.6° to 2.4–14.3° until the end of the breach process. The lower part of the dam in test B1 remained stable during the whole process (Fig. 7) because the gravel content of this dam (76.55 %) was close to the values of stable dams in tests C1–C3 (83.14–88.22 %).

Dams in tests B5 and B6 with fines contents higher than 15 % breached by headcutting along with backward erosion (Figs. 8(b), S8, and S9). A scour pit and then a step-pool structure were formed at the downstream dam slope because the small grains were more easily washed away than the coarse grains. The water flow steepened the breach channel in the downstream slope from a slope angle of 26.6° to nearly vertical due to erosion at the foot of the dam downstream caused

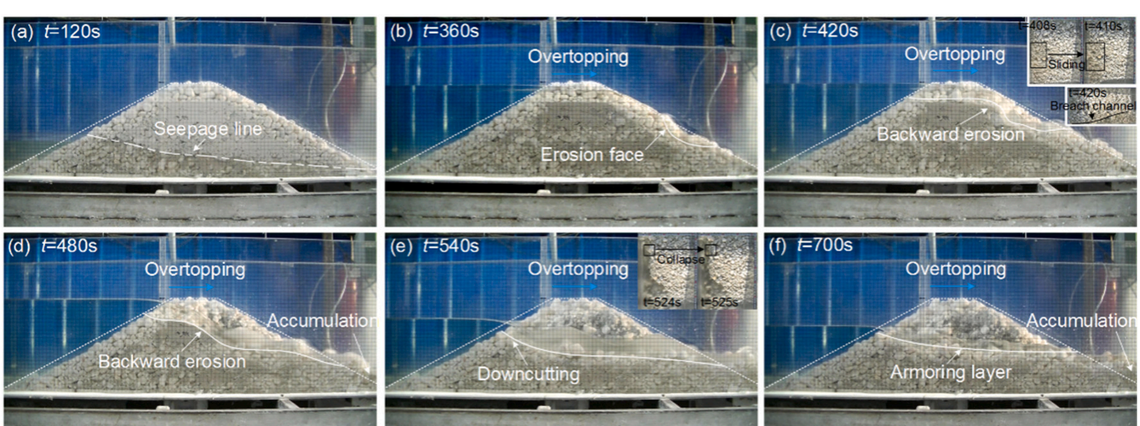

Fig. 7. Failure process of the balanced-composition dam in test B1.

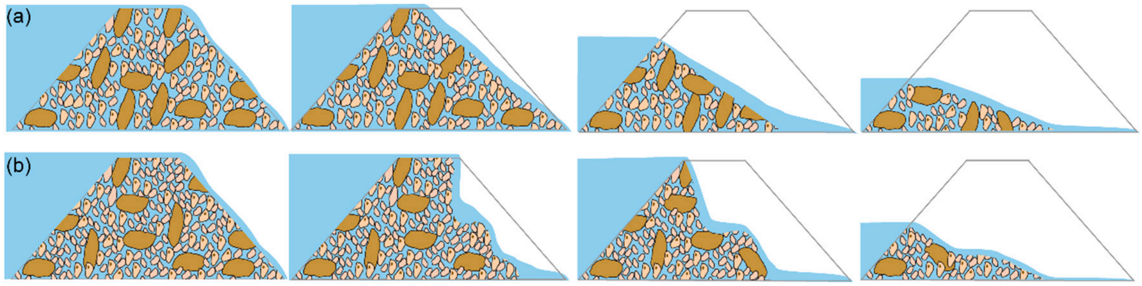

Fig. 8. Schematic illustrations of the longitudinal evolution of balanced-composition dams: (a) tests B1–B4; (b) tests B5 and B6.

by vortexes in the scour pit (Zhu et al., 2020; Zhong et al., 2021). Piping began to form at the toe of the upstream dam face. Headcutting erosion changed to backward erosion when the dam crest disappeared, and the downstream slope angle decreased. This breach process had similarities to tests F1 and F2. The fines contents of dams in tests B5 and B6 (15.53–17.90 %) were much higher than those in tests B1–B4 (1.02–4.56 %), but lower than those in tests F1 and F2 (50.82–55.86 %). This resulted in headcutting erosion of dams in tests B5 and B6: similar to tests F1 and F2, but piping channels were not completely formed during the breach process (Table 1).

3.2.2. Cross-section evolution

The cross-section at the middle of the dam crest was analyzed. For each dam with a fines content <5 % (B1–B4), the bottom of the breach was eroded by the outflow water after initial breach, whereas the top width of the breach expanded slightly (Fig. 9(a)). The width:depth ratio of the breach gradually decreased from 1.25 to 0.52–0.71. Then, the breach side slope began to slip and collapse under gravity because the side slope became larger than the angle of repose of debris. The rate of lateral expansion was higher than that of vertical expansion, resulting in an increase of the width:depth ratio of the breach. The final shape of the breach was almost trapezoidal with a width:depth ratio of 0.73–1.12 (Figs. 9(b) and S10). The final angle of the side slope was in the range 60.1–75.9°: much larger than the angle of repose of the dam material (31.3–38.3°) owing to the apparent cohesion produced by capillary forces (Zhong et al., 2021).

By contrast, the breach channel of each balanced-composition dam with a fines content higher than 15 % (B5 and B6) was widened after overtopping as the dam material slumped from the breach side slope (Fig. 9(a)). The blocks lodged in the breach channel and were progressively eroded. The width:depth ratio rapidly increased to a maximum of 2.15 and 2.44 in tests B5 and B6, respectively. Thereafter, the bottom of the breach was eroded until the shear stress applied by the outflow water was smaller than the resistance shear stress of dam material (1.31 Pa and 1.21 Pa) (Zhou et al., 2019). The width:depth ratio of the breach decreased to the final ratios of 0.86 and 0.69 (Figs. 9(b) and S10). The final side slope angles were 65.8° and 80.3° because the dams contained a large amount of silt so the cohesive force and viscous resistance were large in the unsaturated state (Jiang et al., 2018).

3.3. Effects of grain composition on breach parameters

3.3.1. Dam longevity

The longevity of a dam is defined as the period elapsed from its formation to the end of its failure (Shen et al., 2020). The longevity of fines-dominated dams in tests F1 and F2 (1321–1610 s) were significantly longer than balanced-composition dams in tests B1–B6 (436–605 s) because of the small backward erosion rate in the longitudinal direction and slow development of piping. The longevity of dams with fines contents higher than 15 % in tests B5 and B6 (557–575 s) were longer than those with fines contents <5 % in tests B2–B4 (436–480 s) due to the migration of headcutting.

The longevity of the fines-dominated and balanced-composition dams first decreased and then increased with increasing median diameter d_{50} (Fig. 10(a)). The longevity was influenced by d_{50} because the coarse grain content first decreased and then increased with increasing d_{50}. A large critical shear stress was generated because the large fraction of coarse grains interlocked with each other and formed a skeleton. The dam longevity increased nonlinearly with increasing fines content p (Fig. 10(b)). The reason was that when $p > 25$ %, fines had a cementation effect on the grains, which enhanced the tensile strength and cohesive strength and thus lowered the erodibility of dam material (Vallejo and Mawby, 2000). Dam material with a low proportion of fines and gravel largely consisted of sand in this study which was easily

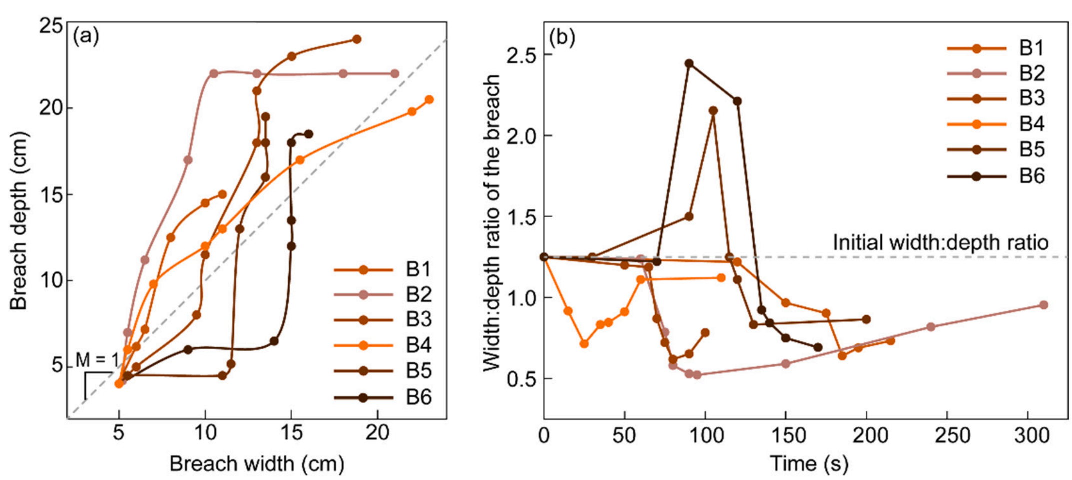

Fig. 9. Relationship between the breach width and depth for dams in tests B1–B6: (a) Relationship between the breach width and depth; (b) Variation of the width:depth ratio during the breach process. Note: M is the gradient.

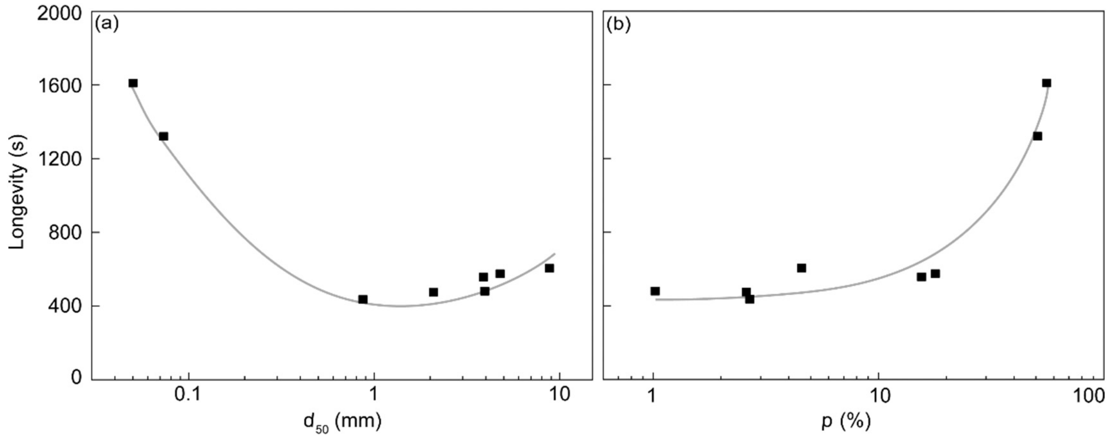

Fig. 10. Relationships between longevity and (a) median diameter d_{50}; (b) fines content p.

eroded. For instance, the dam in test B4 only consisted of sand, showed obvious single-grain movement during the breach process, and had the shortest longevity (436 s) of all balanced-composition dams.

3.3.2. Breach discharge

3.3.2.1. Breach discharge hydrographs. The breach discharge hydrographs of dams with different grain compositions were asymmetrical, and could be divided into four stages, termed initiation, acceleration, attenuation, and rebalance (Fig. 11). In the initiation stage, the breach discharge increased slowly until it almost matched the inflow rate of 1 L/s. The breach discharges in this stage showed fluctuations of 0.3–0.5 L/s in tests F2, B1–B3, and B5–B6 compared with fluctuations of 0.1–0.15 L/s in tests F1 and B4 due to the movement of coarse grains in the breach bottom. The durations of the initiation stage for tests F1 and F2 were 550 s and 265 s, respectively: much longer than for tests B1–B6

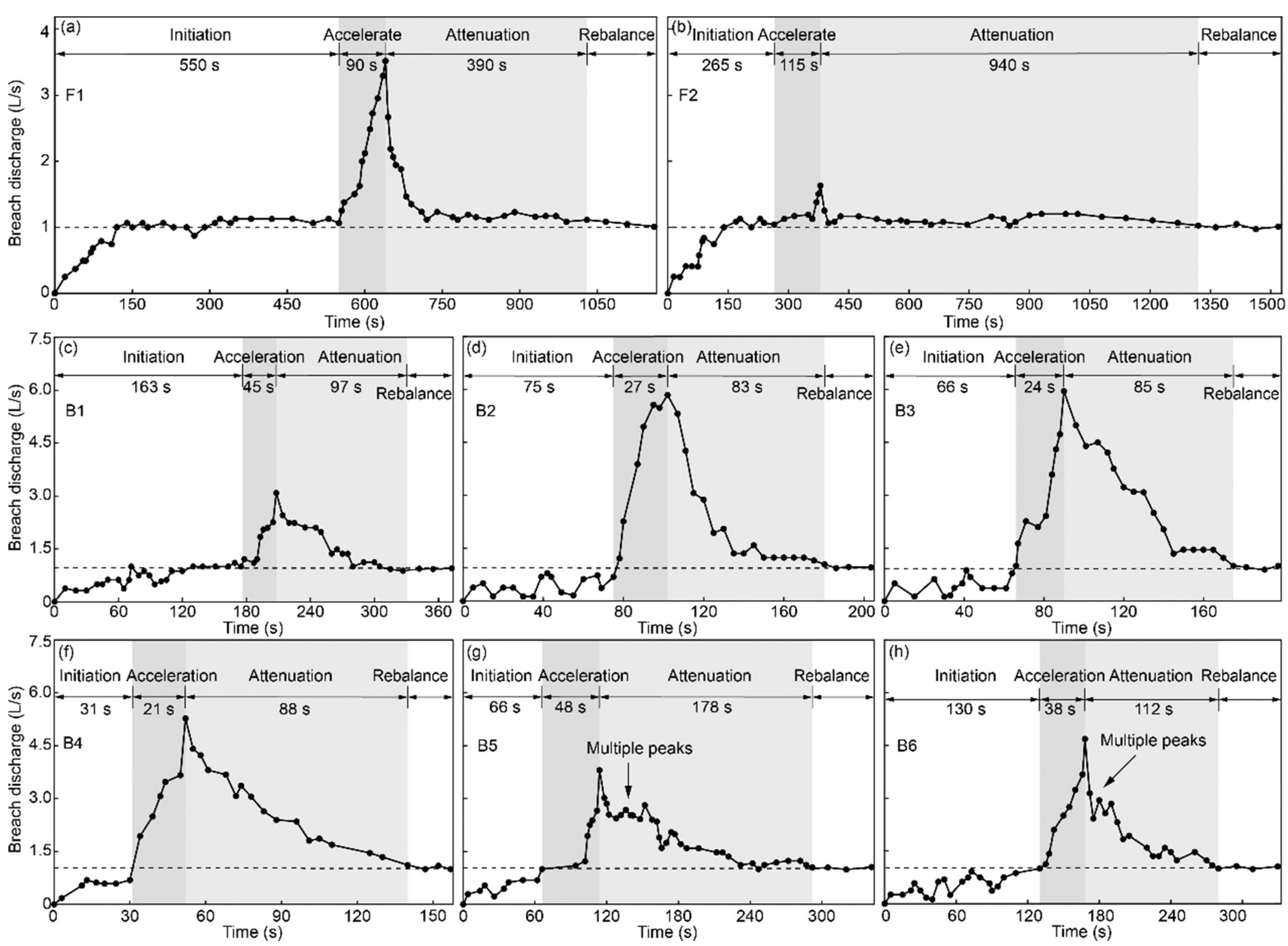

Fig. 11. Breach discharge hydrographs of the fines-dominated and balanced-composition dams.

due to the incomplete development of piping channels. By contrast, the initiation duration for test B4 was the shortest among the tests (31 s) (Fig. 11(f)). The reason was the erodibility of the dam material in test B4 was high as it contained 100 % sand grains. In the acceleration stage, the breach discharge increased rapidly and reached a peak value. The acceleration durations for tests F1 and F2 were also longer than for tests B1–B6 because of the slow enlargement of piping channels along the dam lengths. In the attenuation stage, the breach discharge decreased continuously. In tests F1 and F2, the breach discharge first dropped quickly to small values of 1.1 L/s and 1.08 L/s within 80 s and 20 s, and then slowly declined to stable values in 310 s and 920 s as the piping erosion changed to surface erosion (Figs. 11(a), (b)). In tests B5 and B6, the breach discharge hydrographs had multiple peaks. The primary reason was the side slope collapses with large volumes blocked the breach channels, and the breach discharges decreased until the blockages were scattered and washed away. The outflow water then continued to incise the breaches and later additional peak discharges occurred. The attenuation durations were in the range 83–940 s. Finally, a breach discharge stabilized at the inflow rate in the rebalance stage.

3.3.2.2. Peak discharge. Fig. 12 reflects the relationship between the dam material parameters and peak discharge Q_p. The values of Q_p first increased and then decreased with increasing d_{50} (Fig. 12(a)). The maximum Q_p was 5.95 L/s for the dam with $d_{50} = 2.08$ mm (test B3), while the minimum Q_p was 1.63 L/s for the dam with $d_{50} = 0.05$ mm (test F2). The values of Q_p were small for the fines-dominated dams because the dams failed by overtopping along with piping in this study and the development of piping was slow. For the balanced-composition dams, Q_p decreased with increasing d_{50} due to the increased proportion of coarse grains, which enhanced the connection between grains and increased the erosion resistance. In addition, Q_p decreased with increasing p (Fig. 12(b)). The reason was that dams with high fines contents generally had large cohesive forces and viscous resistances in an unsaturated state, which was proved by the nearly vertical downstream slope face during the breach process (Figs. S8 and S9).

3.3.3. Residual dam height and breach degree

Landslide dams are not completely carried away due to their massive volumes and the presence of low-erodibility debris like large cobbles. The residual dam height h_r is defined as the vertical altitude difference from the valley floor to the highest point on the residual landslide dam. h_r of the fines-dominated and balanced-composition dams in tests F1, F2, and B1–B6 were 2.5–12.2 cm; these first decreased and then increased with increasing d_{50} (Fig. 13). For the fines-dominated dams, the maximum grain diameters in tests F1 and F2 were 5 mm and 40 mm, respectively. During the breach process, more gravel grains were deposited near the dam site in test F2, which prevented further erosion and formed a larger residual dam. For the balanced-composition dams, the gravel content increased with increasing d_{50}, resulting in the larger accumulation of coarse grains in the downstream dam site, the formation of an armoring layer on the dam surface, and thus a higher residual dam height. In addition, the final downstream slope angle β determined the shape of the residual dam. For this study, β values were in the range 2.0–14.3°, and first decreased and then increased with increasing d_{50} due to the change of repose angles of the dam material (Fig. 13).

The destructive power of a landslide dam is not only determined by the lake volume and dam height, but also by the breach degree B_d. B_d is defined as the ratio of the releasing potential energy to the total potential energy of the lake upstream of the landslide dam, where the releasing potential energy is the total potential energy minus the residual potential energy after dam breach.

$$B_d = \frac{m_l g H_d - m_r g h_r}{m_l g H_d} = \frac{\rho_w V_l g H_d - \rho_w V_r g h_r}{\rho_w V_l g H_d} = \frac{V_l H_d - V_r h_r}{V_l H_d} \tag{11}$$

where m_l, V_l and H_d are the mass of the dammed lake water, lake volume and dam height of the original landslide dam. m_r, V_r and h_r are the mass of dammed lake water, lake volume and the dam height of the residual dam. $B_d = 1$ means fully breaching a dam; $B_d = 0$ means no breaching occurs for a dam.

With increasing d_{50}, B_d first increased and then decreased for the fines-dominated and balanced-composition dams since the residual dam height first decreased and then increased (Fig. 14(a)). B_d decreased with increasing gravel content because gravel grains were more difficult to

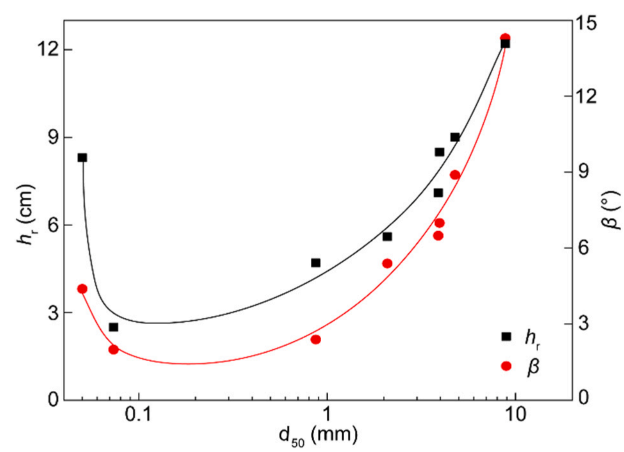

Fig. 13. Relationship between residual dam height h_r, downstream slope angle β and median diameter d_{50}.

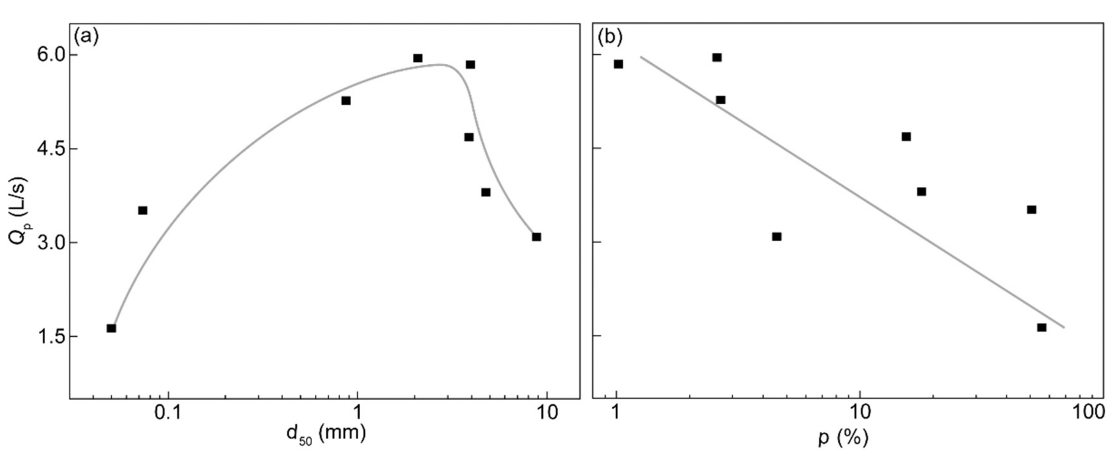

Fig. 12. Relationship between peak discharge Q_p and (a) median diameter d_{50}; (b) fines content p.

wash away than small grains and were easily deposited to form an armoring layer, preventing further erosion (Fig. 14(b)).

4. Discussion

4.1. Stability evaluation of dams

At present, the rapid evaluation of a dam's stability is mainly based on geometric parameters of the dam like the dam height and dam volume, and hydrological parameters of the dammed lake like catchment area and lake volume (Canuti et al., 1998; Ermini and Casagli, 2003; Korup, 2004). It has been suggested that the Backstow Index ($I_s = \log(H_d^3/V_l)$), proposed by Korup (2004), is used to evaluate a dam's stability. However, the stability of landslide dams is difficult to discern with $-3 < I_s < 0$. This includes most of the landslide dams in Appendix 1. The results also show "uncertain" when I_s is applied to evaluate dam stability in this study (Table 2). In practice, the coarse-dominated dams remain stable, while the fines-dominated and balanced-composition dams breach during the experimental process. This indicates that the evaluation of dam stability needs to be further improved by considering grain composition.

The median diameter d_{50} was found to significantly influence the stability of dams (Zhang et al., 2019; Zhu et al., 2020). With increasing d_{50}, dam stability increased and the failure modes changed from overtopping along with piping, to overtopping alone, to remaining stable (Fig. 15(a)). A database of 26 landslide dams was collected to further classify dam stability (Jiang, 2018; Zhang et al., 2016) (Appendix 1). With $-3 < I_s < 0$, the stability of dams depended on d_{50} of the dam material (Fig. 15(b)). When $\log(d_{50}) < 0.9$ mm, the dam was mainly composed of grains with diameters <8 mm, and the dam was in an unstable state. By contrast, when $\log(d_{50}) > 2.0$ mm, the dam was mainly composed of coarse cobbles, and the dam was in a stable state. In cases where 0.9 mm $< \log(d_{50}) <$ 2.0 mm, the dam's stability was uncertain.

4.2. Erodibility of balanced-composition dams

The overtopping of landslide dams depends on the erodibility of dam material, and it is directly affected by the shear stress at the soil/water interface τ.

$$\tau = \frac{\rho_w g n^2 {u_b}^2}{h^{1/3}} \tag{12}$$

where h is the average flow depth. n is the Manning coefficient which is related to d_{50} (Zhou et al., 2019):

$$n = \frac{d_{50}^{1/6}}{A_n} \tag{13}$$

where A_n is an empirical coefficient. Modeling shows that $A_n = 16$ at the laboratory scale (Zhou et al., 2019).

The erosion rate E and shear stress τ at the middle section of the dam crest were calculated and used to analyze the relationship between E and τ. For the balanced-composition dams, E was linearly correlated with τ (Fig. 16), following the relationship proposed by Graf (1984):

$$E = k_d(\tau - \tau_c) \tag{14}$$

where k_d is the coefficient of erodibility (mm^3/N·s), representing how fast the soil is eroded. τ_c is the critical shear stress at the initiation of soil erosion (Pa).

Both τ_c and k_d are obtained based on Eq. 14. The values of τ_c were in the range 0.53–2.16 Pa, and those of k_d were in the range 0.48–1.00 mm^3/N·s. τ_c increased linearly with increasing d_{50}, which was consistent with the equation proposed by Briaud (2008). However, there is no relationship between k_d and d_{50} (Fig. 17).

The breach process of dams is controlled by the change of τ, τ_c, and k_d. The maximum τ in test B1 during the breach process was 10.00 Pa, while the values in tests B2–B6 were in the range 11.25–28.30 Pa. The relatively small τ and large τ_c led to a long breach duration (305 s) and a large residual dam height (12.20 cm) in test B1. By contrast, the maximum τ and k_d in test B4 were 11.25 Pa and 1.00 mm^3/N·s, while τ_c (0.53 Pa) was only 25 % of that in test B1 (2.16 Pa), resulting in a breach duration (140 s) and residual dam height (4.70 cm) less than half of those in test B1. Although the maximum τ was larger than 18.00 Pa in test B5, k_d is 0.48 mm^3/N·s – smaller than the value in test B4 – and thus the breach duration (292 s) was higher than in test B4 (Fig. 11).

4.3. Comparison of stability and breach process of experimental dams with natural landslide dams

In this study, the dams with a high gravel content (>80 %) remained stable with seepage, while the dams with a high fines content (50.82–55.86 %) breached by overtopping along with piping. This result was consistent with the observations of landslide dams in the field. For instance, the Usoi landslide dam, which was composed of a heterogeneous mass of large blocks of rock in the uppermost 50–70 m, had an average inflow rate of 50 m^3/s. The dam remained stable with an average seepage rate of 45.8–47.0 m^3/s since 1911 (Strom, 2010). Conversely, the dam material of the Castle Lake landslide dam was poorly sorted with a median diameter of 0.5 mm, and contained >66.9 % of clay, silt, and sand. This dam failed by piping and overtopping (Meyer et al., 1994).

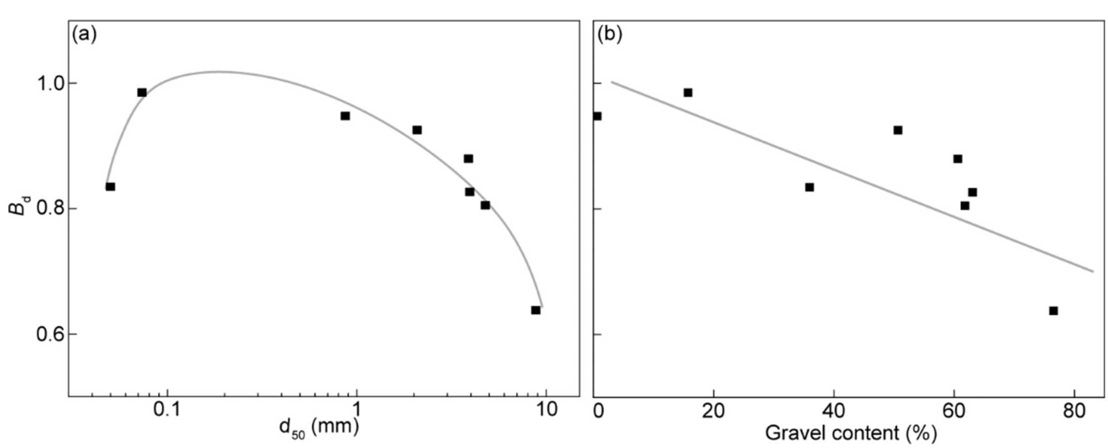

Fig. 14. Relationship between breach degree B_d and (a) median diameter d_{50}; (b) gravel content.

Table 2
Stability evaluation of dams based on Backstow Index (I_s).

Index	Equation	Stable	Uncertain	Unstable	This study	Reference
Backstow Index (I_s)	$\log(H_d^3/V_l)$	>0	−3–0	<−3	−1.23	Korup, 2004

Note: H_d is the dam height. V_l is the lake volume.

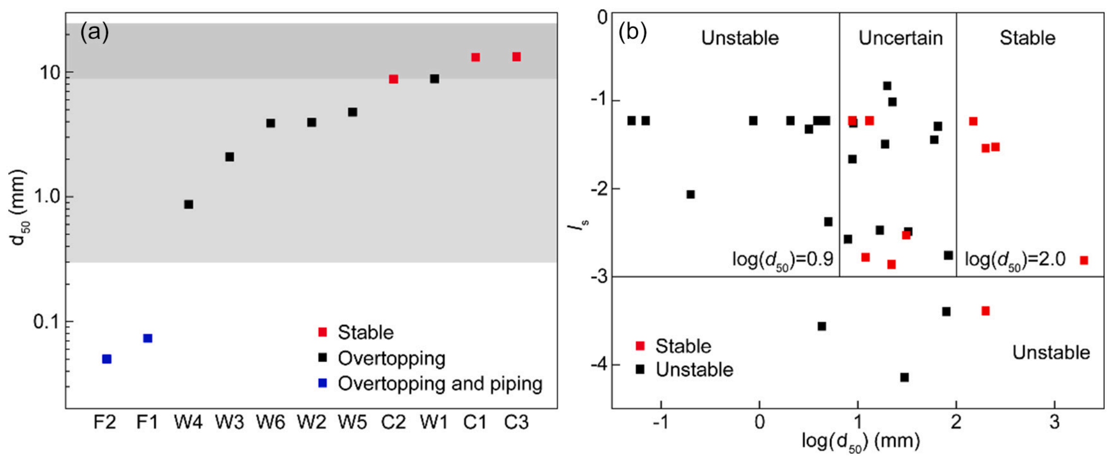

Fig. 15. Effects of median diameter d_{50} of the dam material on the stability of dams: (a) Relationship between d_{50} and dam stability in this study; (b) Improvement of the Backstow Index I_s.

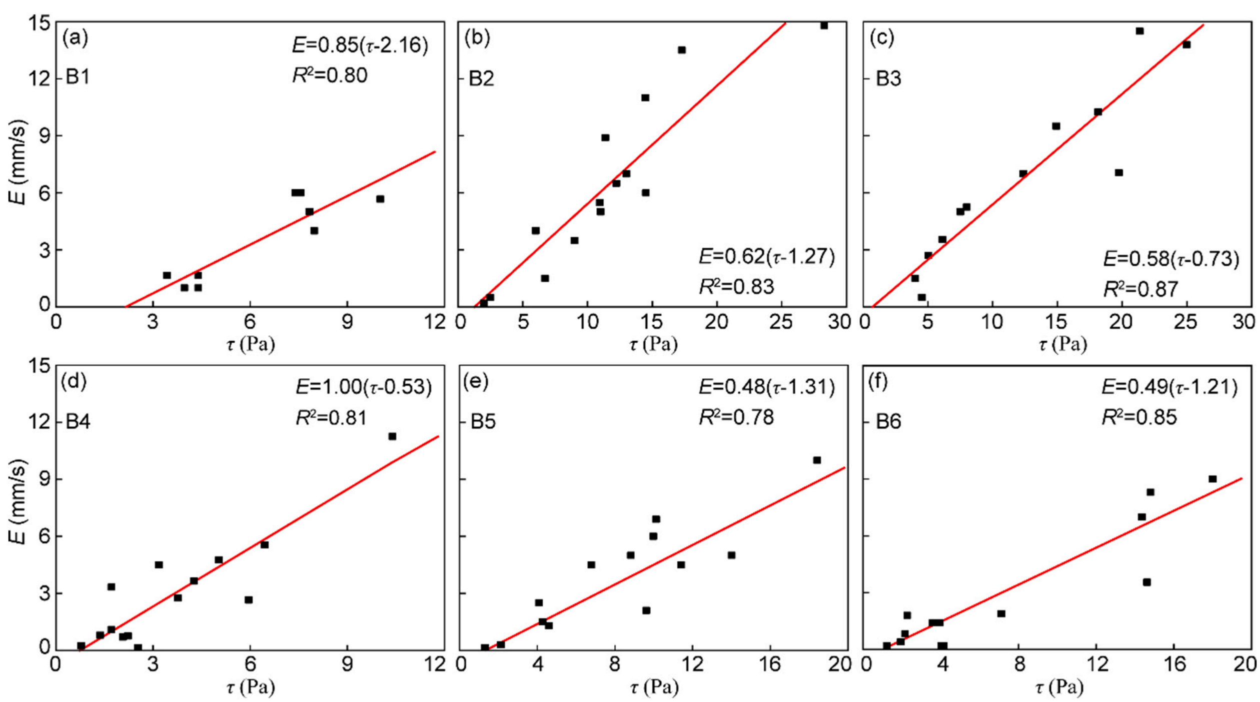

Fig. 16. Correlation between erosion rate E and shear stress τ.

The breach process of a natural landslide dam which fails by piping has seldom been observed and documented as the piping generally occurs in the dam body (Zhong et al., 2021). Therefore, the overtopping process of dams was compared with a natural landslide dam. The Baige landslide dam, with a fines content of 2.0 %, had a dam height of 96 m, a dam bottom width of 1500 m, and an inflow rate of 800 m^3/s. According to Zhong et al. (2021), the breach process of the Baige landslide dam was divided into three stages: (1) Uniform erosion occurred on the surface layer. (2) Backward erosion continued until it reached the dam's upstream face. (3) The breach channel widened and deepened, accompanied by collapse of the breach side slope. The overtopping process of dams with fines contents <5 % in tests B1–B4 was simplified as backward erosion, and the reduction of dam height combined with the widening of the breach channel. The breach process presented similar characteristics to the natural observations.

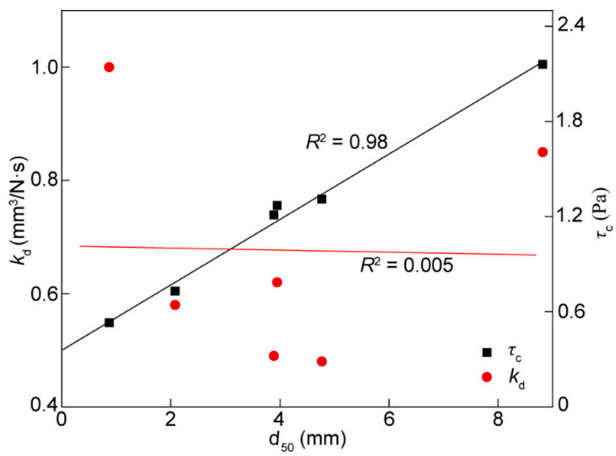

Fig. 17. Relationship between coefficient of erodibility k_d, critical shear stress τ_c and median diameter d_{50}.

4.4. Applicability and limitations of comparing experimental results to natural landslide dams

4.4.1. Applicability of experimental results

The methodology for scaling findings from the experiments to prototype conditions assumes geometric, kinematic and dynamic similarity. Geometric similarity is given by the ratio of the natural landslide dam height H_d* and model dam height H_d conditions:

$$\lambda = \frac{H_d^*}{H_d} = 250 \tag{15}$$

The Froude scaling concept is applied in experiments to maintain dynamic flow similarity (Coleman et al., 2002):

$$F_r = \frac{u_b^*}{\sqrt{gH^*}} = \frac{u_b}{\sqrt{gH}} \tag{16}$$

where u_b* and u_b are the prototype and laboratory flow velocities, respectively. H* and H are the prototype and laboratory hydraulic depths, respectively.

Froude numbers F_r of the outflow water measured in our experiments were varied in the range 0.3–3.5. The selected laboratory and prototype parameters for this study, satisfying Froude scaling and based on the characteristic geometric scale, were compared (Table 3). The natural landslide dams and the model dams are similar under gravity when the Froude numbers of natural landslide dams are equal to those of model dams.

The Reynolds number changed from 483 to 139682 in experiments. The outflow water changed from laminar flow to turbulent flow after dam overtopping in experiments, which was similar to the breach of natural landslide dams (Zhang et al., 2019). During dam breaching, the incipient velocity of grains was obtained based on Wang et al. (2015):

$$U_c = 1.14\sqrt{\frac{\rho_s - \rho_w}{\rho_w} gd}\left(\frac{h}{d}\right)^{1/6} \tag{17}$$

Assuming $h = 0.01$ m in the experiment, the incipient velocity of a grain with a diameter of 1 cm is 0.46 m/s, and the Froude number is 1.47. According to the Froude scaling law, the flow velocity is 7.27 m/s for a natural landslide dam. The radii of grains that can be moved is 1.26 m at a flow velocity of 7.27 m/s.

Table 3
Range of laboratory and prototype parameters for the experiments of this study.

Parameters	H_d (m)	W_t (m)	W_d (m)	H (m)	u_b (m/s)	F_r
Laboratory	0.24	0.12	1.08	0.005–0.04	0.1–1.5	0.3–3.5
Prototype	60	30	270	1.25–10.00	1.6–23.7	0.3–3.5

4.4.2. Limitations of experimental results

The grading curves in this study were chosen based on natural landslide dams in the Northern Apennines, which mainly formed by debris avalanches and debris landslides (Casagli et al., 2003). The model dams thus had a relatively uniform grain-size composition with gravel-sized particles as well as finer material (Zheng et al., 2021b). However, dams formed by rock avalanches usually have a dual structure with crushed debris inside covered by blocky carapace, which may affect breach process. The inflow rate also plays an important role in dam failure modes and breach processes. The inflow rate was maintained at 1 L/s in this study, while the inflow rate of natural landslide dams varies greatly. The influences of dam structure and inflow rate on the breach process and breach parameters certainly merit further investigation in the future.

5. Conclusions

We investigated the breach process of landslide dams through a series of experiments by considering grain compositions. In particular, we discerned the failure modes and evaluated the relationship between dam longevity, breach discharge, and breach degree and dam material parameters.

(1) The stability of dams is influenced by the shear strength of dam material and hydraulic gradient. Coarse-dominated dams remain stable with seepage, fines-dominated dams fail by overtopping along with piping, and balanced-composition dams fail by overtopping alone. The dam stability increases with increasing median diameter. The evaluation of dam stability is further improved by considering the median diameter of debris.
(2) During overtopping processes, the backward erosion is maintained with the reduction of dam height at the longitudinal section, and the width:depth ratio of the breach cross section decreases first and then increases for dams with fines contents <5 %. By contrast, for dams with fines contents larger than 15 %, headcutting erosion causes the development of a step-pool structure and the width:depth ratio increases first and then decreases.
(3) The longevity of dams first decreases and then increases with increasing median diameter, and nonlinearly increases with increasing fines content. The main reason is the grain composition determines the erosion rate and changes the breach duration. The durations of initiation and acceleration stages are longer for fines-dominated dams due to the slow development of piping. The peak discharge first increases then decreases with increasing median diameter. Multiple peaks in a discharge hydrograph may be generated by increasing the fines content or the collapse of the side slope.
(4) Both the residual dam height and final downstream slope angle first decrease and then increase with increasing median diameter due to the change of gravel content and angle of repose of dam material. The breach degree is defined as the ratio of the releasing energy to the total potential energy of the lake upstream of the landslide dam. The breach degree first increases and then decreases with increasing median diameter, and decreases with increasing gravel content.

The results suggest that grain composition of debris has a significant influence on the stability, breach process, and breach parameters of landslide dams. These experimental results can provide guidance for hazard assessment of landslide dams. More landslide dam cases will be collected to validate the improved evaluation method of dam stability, and the influences of dam structure and inflow rate will be further studied in the future.

Declaration of competing interest

The authors declare that they have no known competing financial interests or personal relationships that could have appeared to influence the work reported in this paper.

Acknowledgments

We acknowledge funding from the Natural Science Foundation of China (No. 41731283 and 42007252).

Notation

B_d	breach degree
C_c	curvature coefficient
C_D	drag coefficient
C_L	lift coefficient
C_u	uniformity coefficient
d	diameter of the grain
d_m	maximum diameter of the grain
d_{50}	median grain size of dam material
E	soil erosion rate
e	void ratio of dam material
g	gravitational acceleration
h	average flow depth
H	hydraulic depth
h_b	initial depth of the notch
H_d	dam height
h_r	residual dam height after dam failure
H_w	upstream water level
i	hydraulic gradient
i_c	critical hydraulic gradient
k	saturated permeability coefficient
k_d	coefficient of erodibility
L_d	dam length
L_u	distance from the upstream dam site to the water tank
m_i	mass of the dammed lake water before dam breach
m_r	mass of the dammed lake water after dam breach
n	Manning coefficient
p	fines content (grains smaller than 0.075 mm)
Q_{in}	inflow rate
Q_p	peak discharge
u_b	effective velocity acting on the grain
V_d	dam volume
V_l	lake volume
V_r	residual lake volume after dam failure
w_b	initial top width of the notch
W_d	dam bottom width
W_l	length of the water tank
W_w	width of the water tank
W_f	width of flume
W_t	dam crest width
α	angle between the seepage force and the horizontal
β	angle of downstream slope of the dam
ζ	static friction coefficient.
ρ_w	density of water
ρ_{dmax}	maximum dry density of dam material
ρ_s	density of the grain
τ	shear stress at the soil/water interface
τ_c	critical shear stress
φ	angle of repose of dam material

Appendix A. Supplementary data

Supplementary data to this article can be found online at https://doi.org/10.1016/j.geomorph.2022.108362.

References

Briaud, J.L., 2008. Erodibility of fine grained soils and new soil test. In: Erosion of Soils and Scour of Foundations, 135, pp. 1–10.

Canuti, P., Casagli, N., Ermini, L., 1998. Inventory of landslide dams in the Northern Apennine as a model for induced flood hazard forecasting. In: Andah, K. (Ed.), CNR-GNDCI-UNESCO (IHP): Managing Hydro-Geological Disasters in a Vulnerable Environment for Sustainable Development, Publ. No. 1900 CNR-GNDCI, pp. 189–202.

Casagli, N., Ermini, L., Rosati, G., 2003. Determining grain size distribution of material composing landslide dams in the Northern Apennine: sampling and processing methods. Eng. Geol. 69 (1), 83–97. https://doi.org/10.1016/S0013-7952(02)00249-1.

Chang, D.S., Zhang, L.M., 2010. Simulation of the erosion process of landslide dams due to overtopping considering variations in soil erodibility along depth. Nat. Hazards Earth Syst. Sci. 10 (4), 933–946. https://doi.org/10.5194/nhess-10-933-2010.

Chen, S.C., Lin, T.W., Chen, C.Y., 2015. Modeling of natural dam failure modes and downstream riverbed morphological changes with different dam materials in a flume test. Eng. Geol. 188, 148–158. https://doi.org/10.1016/j.enggeo.2015.01.016.

Chen, S.J., Chen, Z.Y., Tao, R., Yu, S., Xu, W.J., Zhou, X.B., Zhou, Z.D., 2018. Emergency response and back analysis of the failures of earthquake triggered cascade landslide dams on the Mianyuan River, China. Nat. Hazard. Rev. 19 (3), 05018005 https://doi.org/10.1061/(ASCE)NH.1527-6996.0000285.

Coleman, S.E., Andrews, D.P., Webby, M.G., 2002. Overtopping breaching of noncohesive homogeneous embankments. J. Hydraul. Eng. ASCE 128 (9), 829–838. https://doi.org/10.1061/(ASCE)0733-9429(2002)128:9(829).

Dong, J.J., Tung, Y.H., Chen, C.C., Liao, J.J., Pan, Y.W., 2009. Discriminant analysis of the geomorphic characteristics and stability of landslide dams. Geomorphology 110 (3–4), 162–171. https://doi.org/10.1016/j.geomorph.2009.04.004.

Ermini, L., Casagli, N., 2003. Prediction of the behaviour of landslide dams using a geomorphological dimensionless index. Earth Surf. Process. Landf. 28 (1), 31–47. https://doi.org/10.1002/esp.424.

Fan, X.M., Tang, C.X., Westen, J.V., Alkema, D., 2012. Simulating dam-breach flood scenarios of the Tangjiashan landslide dam induced by the Wenchuan Earthquake. Nat. Hazards Earth Syst. Sci. 12 (10), 3031–3044. https://doi.org/10.5194/nhess-12-3031-2012.

Goren, L., Aharonov, E., Sparks, D., Toussaint, R., 2010. Pore pressure evolution in deforming granular material: a general formulation and the infinitely stiff approximation. J. Geophys. Res. Solid Earth 115, B09216. https://doi.org/10.1029/2009JB007191.

Graf, W.H., 1984. In: Hydraulics of Sediment Transport. Water Resources Publications, Colorado, p. 513.

Jiang, M.Z., 2018. Stability Analysis of Landslide Dams Under Surge Waves. Tongji University. Chinese Master thesis.

Jiang, X.G., Wei, Y.W., 2019. Natural dam breaching due to overtopping: effects of initial soil moisture. Bull. Eng. Geol. Environ. 78 (7), 4821–4831. https://doi.org/10.1007/s10064-018-01441-7.

Jiang, X.G., Huang, J.H., Wei, Y.W., Niu, Z.P., Chen, F.H., Zou, Z.Y., Zhu, Z.Y., 2018. The influence of materials on the breaching process of natural dams. Landslides 15 (2), 243–255. https://doi.org/10.1007/s10346-017-0877-9.

Kenney, T.C., Lau, D., 1985. Internal stability of granular filters. Can. Geotech. J. 22 (2), 215–225. https://doi.org/10.1139/t85-029.

Korup, O., 2004. Geomorphometric characteristics of New Zealand landslide dams. Eng. Geol. 73 (1–2), 13–35. https://doi.org/10.1016/j.enggeo.2003.11.003.

Li, D.Y., Zheng, D.F., Wu, H., Shen, Y.Q., Nian, T.K., 2021. Numerical simulation on the longitudinal breach process of landslide dams using an improved coupled DEM-CFD method. Front. Earth Sci. 9, 673249 https://doi.org/10.3389/feart.2021.673249.

Li, M.H., Sung, R.T., Dong, J.J., Lee, C.T., Chen, C.C., 2011. The formation and breaching of a short-lived landslide dam at Hsiaolin Village, Taiwan — Part II: simulation of debris flow with landslide dam breach. Eng. Geol. 123 (1–2), 60–71. https://doi.org/10.1016/j.enggeo.2011.05.002.

Lu, Y., Lu, Y.J., Chiew, Y.M., 2012. Incipient motion of cohesionless sediments on riverbanks with ground water injection. Int. J. Sediment Res. 27 (1), 111–119. https://doi.org/10.1016/S1001-6279(12)60020-1.

Mei, S.Y., Chen, S.S., Zhong, Q.M., Shan, Y.B., 2021. Effects of grain size distribution on landslide dam breaching—insights from recent cases in China. Front. Earth Sci. 9, 658578 https://doi.org/10.3389/feart.2021.658578.

Meyer, W., Schuster, R.L., Sabol, M.A., 1994. Potential for seepage erosion of landslide dam. J. Geotech. Eng. 120 (7), 1211–1229. https://doi.org/10.1061/(ASCE)0733-9410(1994)120:7(1211).

Ministry of Construction of the People's Republic of China, 2001. Code for Investigation of Geotechnical Engineering. GB 50021-2001, Beijing.

Morris, M., Hanson, G., Hassan, M., 2008. Improving the accuracy of breach modelling: why are we not progressing faster? J. Flood Risk Manage. 1 (3), 150–161.

Okeke, A.C., Wang, F.W., 2016. Hydromechanical constraints on piping failure of landslide dams: an experimental investigation. Geoenviron. Disasters 3 (1), 150–161. https://doi.org/10.1111/j.1753-318X.2008.00017.x.

Peng, M., Zhang, L.M., Chang, D.S., Shi, Z.M., 2014. Engineering risk mitigation measures for the landslide dams induced by the 2008 Wenchuan earthquake. Eng. Geol. 180, 68–84. https://doi.org/10.1016/j.enggeo.2014.03.016.

Rozov, A.L., 2003. Modeling of washout of dams. J. Hydraul. Res. 41 (6), 565–577. https://doi.org/10.1080/00221680309506889.

Ruan, H.C., Chen, H.Y., Li, Y., Chen, J.G., Li, H.B., 2021. Study on the downcutting rate of a debris flow dam based on grain-size distribution. Geomorphology 391, 107891. https://doi.org/10.1016/j.geomorph.2021.107891.

Schmocker, L., Frank, P.J., Hager, W.H., 2014. Overtopping dike-breach: effect of grain size distribution. J. Hydraul. Res. 52 (4), 559–564. https://doi.org/10.1080/00221686.2013.878403.

Shen, D.Y., Shi, Z.M., Peng, M., Zhang, L.M., Jiang, M.Z., 2020. Longevity analysis of landslide dams. Landslides 17 (8), 1797–1821. https://doi.org/10.1007/s10346-020-01386-7.

Shire, T., O'Sullivan, C., Hanley, K.J., Fannin, R.J., 2014. Fabric and effective stress distribution in internally unstable soils. J. Geotech. Geoenviron. 140 (12), 04014072 https://doi.org/10.1061/(ASCE)GT.1943-5606.0001184.

Strom, A., 2010. Landslide dams in Central Asia region. J. Jpn. Landslide Soc. 47 (6), 309–324.

Terzaghi, K., 1929. Effect of minor geologic details on the safety of dams: in geology and engineering for dams and reservoirs. Am. Inst. Min. Metall. Pet. Eng. 215, 31–44.

Tian, D.L., Xie, Q., Fu, X., Zhang, J.H., 2020. Experimental study on the effect of fine contents on internal erosion in natural soil deposits. Bull. Eng. Geol. Environ. 79 (8), 4135–4150. https://doi.org/10.1007/s10064-020-01829-4.

Vallejo, L.E., Mawby, R., 2000. Porosity influence on the shear strength of granular material–clay mixtures. Eng. Geol. 58 (2), 125–136. https://doi.org/10.1016/S0013-7952(00)00051-X.

Wang, F.W., Okeke, A.C., Kogure, T., Sakaia, T., Hayashi, H., 2018. Assessing the internal structure of landslide dams subject to possible piping erosion by means of microtremor chain array and self-potential surveys. Eng. Geol. 234, 11–26. https://doi.org/10.1016/j.enggeo.2017.12.023.

Wang, H., Tang, H.W., Zhao, H.Q., Zhao, X.Y., Lu, S.Q., 2015. Incipient motion of sediment in presence of submerged flexible vegetation. Water Sci. Eng. 8 (1), 63–67. https://doi.org/10.1016/j.wse.2015.01.002.

Yang, Y., Cao, S.Y., Yang, K.J., Li, W.P., 2015. Experimental study of breach process of landslide dams by overtopping and its initiation mechanisms. J. Hydrodyn. 27 (6), 827–883. https://doi.org/10.1016/S1001-6058(15)60550-9.

Zhang, J.Y., Fan, G., Li, B.H., Zhou, J.W., Yang, X.G., 2021. Large-scale field model tests of landslide dam breaching. Eng. Geol. 293, 106322 https://doi.org/10.1016/j.enggeo.2021.106322.

Zhang, L.M., Peng, M., Chang, D.S., Xu, Y., 2016. Dam Failure Mechanisms and Risk Assessment. John Wiley & Sons, Singapore.

Zhang, L.M., Xiao, T., He, J., Chen, C., 2019. Erosion-based analysis of breaching of Baige landslide dams on the Jinsha river, China, in 2018. Landslides 16 (10), 1965–1979. https://doi.org/10.1007/s10346-019-01247-y.

Zhao, T.L., Chen, S.S., Fu, C.J., Zhong, Q.M., 2019. Centrifugal model tests and numerical simulations for barrier dam break due to overtopping. J. Mt. Sci. 16 (3), 630–640. https://doi.org/10.1007/s11629-018-5024-0.

Zheng, H.C., Shi, Z.M., Yu, S.B., Fan, X.M., Hanley, K.J., Feng, S.J., 2021a. Erosion mechanisms of debris flow on the sediment bed. Water Resour. Res. 57 (12), e2021WR030707 https://doi.org/10.1029/2021WR030707.

Zheng, H.C., Shi, Z.M., Shen, D.Y., Peng, M., Hanley, K.J., Ma, C.Y., Zhang, L.M., 2021b. Recent advances in stability and failure mechanisms of landslide dams. Front. Earth Sci. 9, 659935 https://doi.org/10.3389/feart.2021.659935.

Zhong, Q.M., Chen, S.S., Wang, L., Shan, Y.B., 2020. Back analysis of breaching process of Baige landslide dam. Landslides 17 (7), 1681–1692. https://doi.org/10.1007/s10346-020-01398-3.

Zhong, Q.M., Wang, L., Chen, S.S., Chen, Z.Y., Shan, Y.B., Zhang, Q., Ren, Q., Mei, S.Y., Jiang, J.D., Hu, L., Liu, J.X., 2021. Breaches of embankment and landslide dams–State of the art review. Earth Sci. Rev. 216, 103597 https://doi.org/10.1016/j.earscirev.2021.103597.

Zhou, G.D., Zhou, M.J., Shrestha, M.S., Song, D.R., Choi, C.E., Cui, K.F.E., 2019. Experimental investigation on the longitudinal evolution of landslide dam breaching and outburst floods. Geomorphology 334, 29–43. https://doi.org/10.1016/j.geomorph.2019.02.035.

Zhou, Y.C., Xu, B.H., Yu, A.B., Zulli, P., 2002. An experimental and numerical study of the angle of repose of coarse spheres. Powder Technol. 125, 45–54. https://doi.org/10.1016/S0032-5910(01)00520-4.

Zhu, X.H., Peng, J.B., Liu, B.X., Jiang, C., Guo, J., 2020. Influence of textural properties on the failure mode and process of landslide dams. Eng. Geol. 271, 105613 https://doi.org/10.1016/j.enggeo.2020.105613.